Biofabrication

PAPER

Precisely defined fiber scaffolds with 40 μm porosity induce elongation driven M2-like polarization of human macrophages

Tina Tylek[1], **Carina Blum**[1], **Andrei Hrynevich, Katrin Schlegelmilch, Tatjana Schilling, Paul D Dalton and Jürgen Groll**[2]

Department of Functional Materials in Medicine and Dentistry and Bavarian Polymer Institute (BPI), University Hospital of Würzburg, Pleicherwall 2, D-97070 Würzburg, Germany

[1] These authors contributed equally to this work.

[2] Author to whom any correspondence should be addressed.

E-mail: tina.tylek@fmz.uni-wuerzburg.de, carina.blum@fmz.uni-wuerzburg.de, andrei.hrynevich@fmz.uni-wuerzburg.de, katrin.schlegelmilch@fmz.uni-wuerzburg.de, tatjana.schilling@fmz.uni-wuerzburg.de, paul.dalton@fmz.uni-wuerzburg.de and juergen.groll@fmz.uni-wuerzburg.de

Keywords: cell elongation, human macrophages, melt electrowriting (MEW), macrophage polarization, 3D scaffolds

Supplementary material for this article is available online

OPEN ACCESS

RECEIVED
3 October 2019

REVISED
12 November 2019

ACCEPTED FOR PUBLICATION
5 December 2019

PUBLISHED
7 February 2020

Abstract

Macrophages are key players of the innate immune system that can roughly be divided into the pro-inflammatory M1 type and the anti-inflammatory, pro-healing M2 type. While a transient initial pro-inflammatory state is helpful, a prolonged inflammation deteriorates a proper healing and subsequent regeneration. One promising strategy to drive macrophage polarization by biomaterials is precise control over biomaterial geometry. For regenerative approaches, it is of particular interest to identify geometrical parameters that direct human macrophage polarization. For this purpose, we advanced melt electrowriting (MEW) towards the fabrication of fibrous scaffolds with box-shaped pores and precise inter-fiber spacing from 100 μm down to only 40 μm. These scaffolds facilitate primary human macrophage elongation accompanied by differentiation towards the M2 type, which was most pronounced for the smallest pore size of 40 μm. These new findings can be important in helping to design new biomaterials with an enhanced positive impact on tissue regeneration.

1. Introduction

Influencing or ideally directing the innate immune response after implantation remains one of the major challenges in the development of biomaterials and the design of three-dimensional (3D) scaffolds [1]. The early phase of the immune reaction is characterized by protein adsorption to the biomaterial's surface, followed by a provisional matrix formation [2]. The subsequent acute inflammation involves neutrophil recruitment to the injury site from the blood stream. This neutrophil response after biomaterial implantation commonly resolves within several days and overlaps with subsequent arrival of mononuclear cells such as monocytes and lymphocytes that can initiate the chronic inflammatory response at the site of implantation [3]. Thereby, monocyte-derived macrophages are among the key players of the initial inflammatory reaction and overall response to the implanted biomaterial, determining whether a fibrous capsule formation or the resolution of the inflammatory process and hence tissue regeneration will take place [4].

Macrophages are highly plastic and can roughly be divided into two main subtypes depending on their functionality and spatial occurrence: the 'classically activated' M1 and the 'alternatively activated' M2 phenotype [5]. The M1 macrophages typically release high amounts of pro-inflammatory cytokines such as IL-1β, IL-8, and TNFα, show microbicidal activity as well as a high phagocytic activity, and produce reactive nitrogen and oxygen species [6, 7]. This M1 macrophage action always provokes an inflammatory response after biomaterial implantation and is mandatory as an initial step for proper wound healing and tissue regeneration. However, the extended presence of M1 macrophages leads to severe foreign body responses as well as granuloma and fiber encapsulation

resulting in a chronic inflammatory response and failure of the biomaterial's integration [8].

In contrast, M2 macrophages release anti-inflammatory cytokines such as IL-10 and are characterized by the expression of scavenger (CD163) as well as mannose receptors (CD206) [9, 10]. Furthermore, they comprise a range of different subsets (M2a, M2b, M2c) with functionalities ranging from regulation to wound healing [11]. While the M2a and M2b subgroups fulfill immune regulatory functions, the M2c subset is crucial for tissue remodeling and the suppression of inflammatory immune responses by the secretion of TGF-β1 and IL-10 [12, 13]. These factors contribute to the vascularization of regenerative biomaterials and inhibiting the formation of fibrous tissue, which greatly improves the integration and performance of the biomaterial to fulfill its intended function [5].

For tissue-regenerative applications, it is therefore of importance that biomaterials can attenuate the pro-inflammatory response and to promote macrophage polarization into the regenerative type. One strategy to generate immunomodulating biomaterials are (bio) chemical modifications at the material surface. For example, extracellular matrix proteins can be used to control the integrin adhesion of monocytes and thereby either prevent M1 polarization or promote M2 differentiation [14–16]. Furthermore, biomaterials can be designed to present as well as to release anti-inflammatory molecules, such as dexamethasone [17], heparin [18], and cytokines like IL-4 or IL-10 [15, 19, 20], respectively, or to bind pro-inflammatory cytokines by functionalized electrospun fiber surfaces with neutralizing antibodies [21] to modulate the immune response.

Another strategy to influence the immune response involves physical cues, such as material stiffness, surface roughness, topography or microstructure of the biomaterial. Accordingly, stiffer hydrogels promoted macrophage adhesion but also increased the pro-inflammatory immune response compared to softer gels [22]. Furthermore, porous structures have already been described to influence the polarization of macrophages *in vivo* [23]. A concave-structured hydrogel, based on poly(2-hydroxyethyl methacrylate) (pHEMA) with a highly ordered architecture and exactly equally-sized pores of up to 40 μm, showed a pronounced infiltration of murine macrophages being mainly directed towards the healing phenotype. However, the scaffold fabrication method, used in this study, does yield scaffolds with a bimodal pore size distribution, originating from the diameter of the templating spheres and their contact areas in dense packing. Hence, an unambiguous correlation between a defined pore size and effects on innate immune cells is difficult.

Also, extrusion-printed porous scaffolds of chitosan with diagonally orientated fibers generating triangular-like pores with filament diameters of 75 ± 5 μm as well as inter-filament spacings of 165 ± 5 μm, were shown to promote the anti-inflammatory macrophage phenotype. These scaffolds decreased the pro-inflammatory cytokine release of these cells whereas the secretion of pro-inflammatory markers by macrophages on box-shaped constructs with orthogonally arranged fibers was enhanced [24].

In addition, McWorther *et al* (2013), Wang *et al* (2016) as well as Chen *et al* (2010) have reported considerable effects of micro- and nano-topographical features towards the M2 macrophage polarization [25–28], when murine macrophages were triggered to adopt an elongated phenotype by these setups in *vitro* and *in vivo*. While this effect of elongation and the correlation with a thereby induced M2 polarization could be described in 2D for murine macrophages by either micropatterning or stimulation with IL-4 [27], this behavior could so far not be triggered for primary human macrophages. For human macrophages, the induced polarization in 2D by differentiation factors lead to a pronounced elongated shape rather for M1- (LPS/INF-γ) than for M2- (IL-4 or Dexamethasone) macrophages [29, 30]. It has furthermore been shown that the outcome of morphology and polarization of human macrophages differs between 2D and 3D environments [31, 32]. However, the elongation of human monocyte-derived macrophages on 3D scaffolds and the resulting effects on differentiation and polarization has so far been unexplored. One potential reason is the lack of suited scaffold fabrication methods.

The additive manufacturing technique of melt electrowriting (MEW) is an especially suitable and advantageous approach in this context as it enables the production of highly defined scaffold geometries built of fibers with diameters in the lower micrometer range [33]. In detail, defined pore sizes as well as pore interconnectivities have been achieved when directly-written fiber substrates were generated by MEW in a layer-by-layer fashion [34, 35]. Our group has also demonstrated the ability of cells to attach, infiltrate, and proliferate upon seeding onto MEW scaffolds, of interest for various tissue engineering applications [35–37]. The most widely investigated polymer for MEW processing is poly(ε-caprolactone) (PCL), which is compatible with both *in vivo* and *in vitro* applications [38]. Defined melt-electrowritten PCL constructs with pore sizes ranging from several micrometers to several millimeters and fiber diameters between 800 nm and 50 μm [37, 39] have been previously described. The fiber deposition accuracy, is one limitation of MEW, especially with build height [40] and is mainly affected by dielectric shielding and residual charges around each deposited fiber [41]. On the one hand, this limits the discrete deposition of any two fibers to a minimal distance of a few tens of micrometers, depending on the fiber diameter, process parameters and used polymer. On the other hand, this

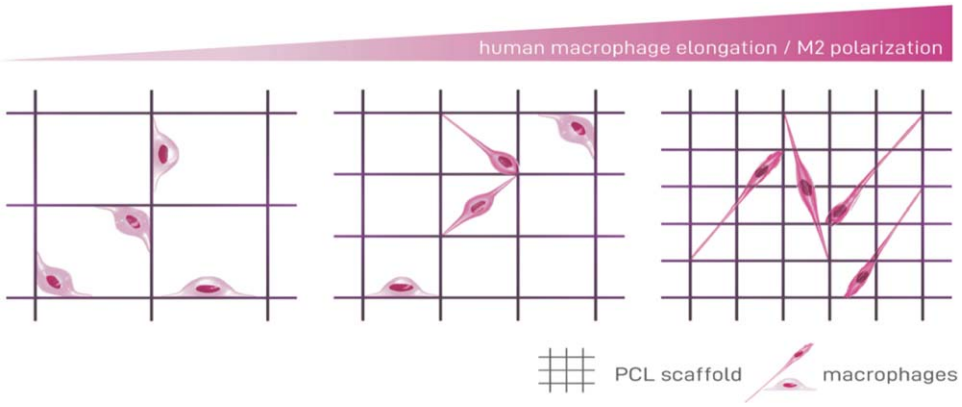

Scheme 1. Smaller pore sizes promote human macrophage elongation and M2-like polarization. Melt-electrowritten fiber scaffolds with decreasing pore sizes enhance the potential of human macrophages to elongate. Furthermore, the elongation is linked to an increased M2-like polarization. Thus, this study demonstrates that 3D design of biomaterials with precisely adjusted porosity is a strategy to modulate the polarization of human macrophages.

Table 1. Manufacturing parameters and settings for the production of box-, triangle-, round-, and disordered MEW scaffolds.

Geometry	Melt temperature (°C)	Nozzle	Air pressure (bar)	Collector distance (mm)	Voltage	Linear collector speed (mm min^{-1})
Square box	85	30G	2	1.4	earth/+4.0 kV	950
Triangle	85	30G	2	1.4	earth/+4.0 kV	950
Round	77	25G	1.2	1.0	−0.5 kV 2.5 kV	70
Disordered	95	22G	0.2	8	−2.5 kV 8.0 kV	100

electrostatic attraction of fibers assists in the precise stacking of fibers to a certain height.

In the present study, we have advanced the precision of MEW to allow for the fabrication of 3D porous fiber scaffolds with several adjustable but defined geometries that comprise one consistent pore size down to 40 μm throughout each individual construct. Box-shaped constructs with pore sizes ranging from 40 to 100 μm were then seeded with primary human peripheral blood derived macrophages. Analysis of the cell behavior on these scaffolds regarding cell morphology, gene expression, cytokine release, surface marker expression and phagocytic activity provided for the first time a clear evidence of elongation driven human macrophage polarization in 3D scaffolds. Specifically, the data shows the correlation between small pore sizes and the cells' increased elongation behavior as well as their enhanced differentiation towards a pro-healing M2 macrophage phenotype (scheme 1). Altogether, this suggested an extended geometry-based healing effect for those 3D scaffolds with the smallest pore size tested and might set the stage for planning future promising biomaterial designs of clinical relevance.

2. Materials and methods

2.1. Materials

Medical-grade PCL (Corbion Inc., Netherlands, PURASORB PC 12, Lot# 1412000249, 03/2015) was used as received and handled as described elsewhere [42]. All other chemicals were purchased from Merck (Darmstadt, Germany) unless otherwise stated.

2.2. 3D PCL MEW scaffold and 2D PCL film fabrication

All samples were fabricated with a previously described, custom-built MEW printer [42]. The main experiments in this study were performed with square box-shaped scaffolds, whose manufacturing parameters slightly differed from scaffolds with other geometries (table 1). Briefly, PCL pellets for box-shaped scaffolds were molten in a syringe with a 30G nozzle (Nordson Deutschland GmbH, Germany) at up to 77 °C until completely liquefied. A positive, 4.0 kV high voltage was applied to the nozzle while the collector plate was grounded. The distance between the nozzle and the collector plate was adjusted to 1.4 mm. The polymer melt was pushed through the nozzle by applying 2 bar air pressure on the entire syringe. MEW head (heater, syringe and nozzle) was held in a fixed position and straight fibers were printed onto a moving collector plate at a speed of 950 mm min^{-1}. After the initial stabilization of the electrified polymer jet, the box-shaped scaffolds (10 mm × 10 mm) were directly written as 3D structures using a similar G-code motion path and filament deposition onto the collector plate as has been previously described [39]. The manufacturing parameters for the triangle-, round-, and disordered-shaped scaffolds were adapted as listed in

Table 2. Combinations of pore size, number of stacked layers, and fiber diameter.

Pore size (μm)	Actual pore size (μm)	Number of layers in x- and y-direction	Fiber diameter (μm)
100	102.9 ± 3.3	2 × 30	2.9 ± 0.3
80	80.7 ± 2.8	2 × 20	2.6 ± 0.3
60	59.5 ± 2.0	2 × 18	2.7 ± 0.2
50	49.8 ± 1.4	2 × 15	2.9 ± 0.2
40	40.0 ± 0.6	2 × 10	2.6 ± 0.2

table 1. The box-shaped scaffolds were further varied and differed in the pore size and the stacking height as stated in table 2.

A smooth PCL film was used as a 2D control, where PCL pellets were melted using a heat gun at a temperature of 90°C. The film was drawn at a speed of 2 mm s^{-1} to a thickness of approximately 100 μm. For the cell culture experiments, PCL film disks with a diameter of 14 mm were used.

Prior to cell culture experiments, PCL MEW scaffolds and films were sterilized in 70 % ethanol for 30 min followed by extensively washing in Dulbecco's phosphate buffered saline (PBS).

2.3. Scaffold imaging and characterization

For the scaffold imaging using a Zeiss Crossbeam 340 scanning electron microscope (SEM; Carl Zeiss Microscopy GmbH, Oberkochen, Germany), the samples were coated with a 3 nm thick conductive platinum layer in a Leica EM ACE600 sputtering unit (Leica Microsystems, Wetzlar, Germany) prior to SEM imaging. The straight-line selection tool of ImageJ software was used to measure pore size (defined as the space between the inner edges of two parallel fibers) and fiber diameters. Measurements were taken at 20 random regions within the SEM images and mean values were calculated.

3. Biological methods

3.1. Cell culture

All experiments were performed with the approval of the Local Ethics Committee of the University of Würzburg. Buffy coats were obtained from the Bavarian Red Cross (Blood donor service, German Red Cross, Wiesentheid, Germany) with the written informed consent of each blood donor.

Monocytes were isolated from human blood-derived buffy coats of healthy donors. Peripheral blood mononuclear cells were collected by density gradient centrifugation with Pancoll (Density: 1077 g l^{-1}; Pan-Biotech, Aidenbach, Germany). Monocytes were isolated via negative selection (Pan Monocyte Isolation Kit, Miltenyi Biotec, Gladbach, Germany). Cells were seeded onto the different scaffold types and the 2D-PCL control and cultivated for up to seven days in macrophage culture medium (RPMI-1640, GlutaMAX™ (Thermo Fischer Scientific, Waltham, USA)) with 10% (v/v) of human platelet lysate [43] (hPL, PL Bioscience, Aachen, Germany) and 1% (v/v) Penicillin-Streptomycin (Pen-Strep; 5000 U ml^{-1}) (Thermo Fisher Scientific, Waltham, USA) in tissue culture-treated 24-well plates (Nunc, Thermo Fischer Scientific, Waltham, USA) in a humidified atmosphere at 37 °C and 5% CO_2. Monocytes differentiated spontaneously, i.e. without supplemented differentiation factors, into so-called M0 macrophages within this time.

In detail, 0.75 × 10^6 freshly isolated monocytes suspended in 50 μl were seeded onto each sample in a tissue culture-treated 24-well plate. While melt-electrowritten scaffolds were subsequently incubated in a humidified atmosphere at 37 °C and 5% CO_2 for 0.5 h to facilitate cell adhesion before additional 1 ml cell culture medium was added, cells on the 2D PCL film were immediately supplied with 1 ml macrophage culture medium. To avoid cell loss, each scaffold and also PCL film was weighed down with a sterile plastic ring cut from a serological pipette (Greiner BioOne, Kremsmünster, Austria) for the first two days of cultivation.

Each experiment was performed at least three times with independent primary donor material (n = 3).

3.2. Molecular methods

3.2.1. Determination of DNA amount

To determine the DNA amount that correlates with the number of adhered macrophages, the Quant-iT™ PicoGreen® dsDNA Reagent and Kit (Thermo Fisher Scientific, Waltham, USA) were used according to the manufacturer's manual employing the middle-range standard curve. In short, macrophages were cultivated on PCL films and scaffolds in 24-well plates in 1 ml macrophage culture medium per well in a humidified atmosphere at 37 °C and 5% CO_2. After one and seven days, cells were washed once with PBS^- and lyzed in 1 ml 1% Triton X-100 in PBS^- for 1 h at 4 °C. The standards and samples were excited at 485 nm and the fluorescence emission intensity was measured at 538 nm on a plate reader (Tecan, Männedorf, Switzerland).

3.2.2. Gene expression analysis

Total cellular RNA of macrophages was isolated using PeqGold Trifast (VWR, Darmstadt, Germany) in accordance with the manufacturer's protocol. Cell-laden scaffolds were placed into a fresh well to exclude any cells having possibly adhered to the cell culture plastic from further analysis. cDNA was generated with the High-Capacity cDNA Reverse Transcription Kit (Thermo Fisher Scientific, Waltham, USA) according to the manufacturer's manual. The mRNA expression levels of macrophages were analyzed via

quantitative Real-Time PCR (qPCR) (StepOnePlus; Thermo Fisher Scientific, Waltham, USA) with SYBR™ Select Master Mix (Thermo Fisher Scientific, Waltham, USA). Each 10 μl qPCR reaction comprised 5 ng of cDNA and 200 nM primer sequences (Biomers, Ulm, Germany) (table S1 is available online at stacks.iop.org/BF/12/025007/mmedia). For each cDNA sample, the threshold cycle (Ct) value of each target sequence was subtracted from the Ct value of the house keeping mRNA RPS27a to derive ΔCt. Gene expression changes were calculated by the $2^{-\Delta\Delta Ct}$ method. A control group of macrophages, as indicated in the figure legends, was used for normalization.

3.2.3. Cytokine quantification via Single-Analyte ELISArray Kits

The cytokine release of spontaneously differentiated macrophages cultivated on 2D PCL films and 3D scaffolds was tested via Single-Analyte ELISArray Kits (Qiagen, Hilden, Germany) after three and seven days of cultivation. The production of IL-1β, IL-8, IL-6, and IL-10 was analyzed in samples' supernatants according to the manufacturer's protocol. Thereby, the absorbance measured on a plate reader (Tecan, Männedorf, Switzerland) at 450 nm and corrected with the absorbance at the reference wavelength of 570 nm directly correlated with the amounts of cytokines. For the normalization to cell numbers, the DNA levels of macrophages on the corresponding scaffolds were determined as described above and taken into account.

3.3. Imaging

3.3.1. SEM sample preparation

For SEM preparation after seven days of cultivation, samples were fixed with 6% glutaraldehyde for 15 min on ice. Then samples were incubated two times with PBS^- on ice prior to their dehydration by a graded ethanol series (2 × 70%, 2 × 90%, 2 × 100% (v/v)). After drying via hexamethyldisilazane, the samples were fixed on stubs and coated as mentioned above. For the determination of the percentage and individual length of elongated cells, 20 random images per donor were taken and analyzed via ImageJ. For this, each cell on the random images were counted, and subsequently, the length of cells, which were elongated and stretched on the walls and/or across the pores were measured using the line tool of ImageJ. Cells that had a roundish, spherical morphology were counted as 'non-elongated'. Afterward, the percentage of elongated cells and the average cell length on the different scaffold types were calculated.

3.3.2. Immunofluorescence staining of cell surface proteins

Macrophages were cultured either on the 2D PCL film or scaffolds for seven days and fixed with 4% formaldehyde for two hours at room temperature (RT). The samples were washed twice with PBS and blocked with 2% bovine serum albumin in PBS^- for 30 min at RT. Primary antibodies against CD163 (#TA506380, OriGene, Rockville, USA; 1:100) and CD206 (#ab64693, Abcam, Cambridge, UK; 1:400) were applied for 2 h at RT in a humidified chamber. Subsequently, fluorescence-labeled secondary antibodies $Cy^{TM}2$-conjugated AffiniPure Goat Anti-Rabbit or $Cy^{TM}3$-conjugated AffiniPure Goat Anti-Mouse (Jackson ImmunoResearch; Dianova, Hamburg, Germany) were applied for 30 min at RT. Samples were washed and mounted 'Immunoselect Antifading Mounting Medium' with DAPI (Dianova, Hamburg, Germany). Images were captured via fluorescence microscopy (Axio Observer, Zeiss equipped with epi fluorescence optics, a MRm camera and a Apotome; Zeiss, Oberkochen, Germany). A Z-stack experiment with 25 images per stack was performed to capture cells throughout the scaffold. The apotome was used to avoid scattered light. After imaging, an overlay of the individual images of the stack was made by imageJ.

3.3.3. Phagocytosis assay

The phagocytic activity of macrophages was analyzed using 2 μm red fluorescence-labeled latex beads (Sigma-Aldrich, Munich, Germany). The beads were added to the macrophage culture in a ratio of 10 beads per seeded cell and incubated in a humidified atmosphere for 2 h at 37 °C and 5% CO_2. Cell-laden 3D scaffolds as well the 2D controls were washed three times with serum-free macrophage culture medium to remove non-phagocytosed beads.

The phagocytotic activity was analyzed via fluorescence microscopy by counting engulfed beads of ten random pictures of each scaffold via image j. To exclude beads attached to the scaffolds themselves, cell-free scaffolds were treated in the same way and the measured beads subtracted from them of the cell-laden scaffolds. For normalization the DNA amount of the macrophages was determined for each scaffold as described above.

3.4. Statistics

Statistica (Statsoft, Hamburg, Germany) was used for statistical analyses. The statistical significance of qPCR data was determined by the two-sample t-test, for all other data, two-way analysis of variance (ANOVA) was performed. Results were considered to be significantly different at a p value below 0.05.

4. Results

4.1. Spontaneous macrophage polarization depends on scaffold geometry

MEW was applied to produce 3D fiber scaffolds made of PCL. The scaffolds differed in their design, i.e. square, triangular, roundish, and disordered

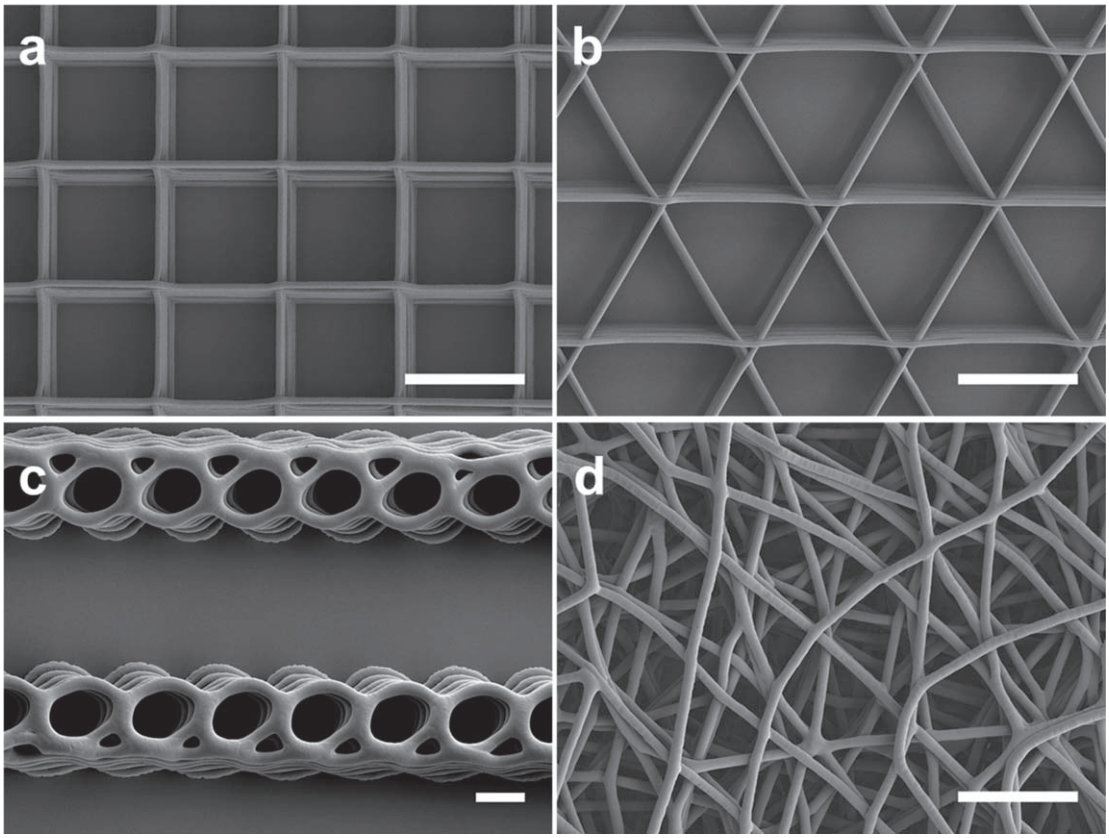

Figure 1. MEW scaffolds with different geometries. (a): box-shaped (50 μm 2 × 15), (b): triangle-shaped (60 μm 3 × 10), (c): round-shaped (5 layers), (d): disordered (2 layers). Scale bar = 50 μm.

geometries were produced (figure 1), which was accompanied, to a certain extent, by different fiber diameters.

The cultivation of monocyte-derived macrophages on MEW scaffolds with different geometries for a period of seven days resulted in different cell morphologies as detected by SEM (figures 2(a)–(d), S2). Whereas macrophages developed an elongated and stretched phenotype across the pores on box-shaped scaffolds (figure 2(a)), their cultivation on triangle-shaped scaffolds (figure 2(b)) led them to adapt the scaffold morphology and to span the gap between adjacent fibers. On round-structured scaffolds, with a larger fiber diameter (around 18 μm) (figure 2(c)), compared to the other geometries (3 μm), macrophages developed no predominantly morphology. Some cells were flattened with complete contact of the material-facing cell surface to individual fibers, while others had developed a rather spherical phenotype and some cells stretched across these roundish pores. After cultivation on randomly structured morphologies (figure 2(d)), macrophages grew into the individual pores spanning several layers of the scaffold. The gene expression profiles detected after seven days of spontaneous differentiation (figure 2(e)) were dependent on the different scaffold geometries. Macrophages cultivated on box-shaped scaffolds showed a stronger down-regulation of the M1 markers IL-1β and IL-8 in parallel with the highest up-regulation of the M2 marker CD163 when compared all other geometries. Scaffolds with a roundish morphology provoked the smallest M1 marker downregulation and a significant decrease of M2-specific CD163 compared to box-shaped and disordered pores. Macrophages cultivated on triangle-shaped scaffold, slightly decreased the IL-8 and slightly increased the CD163 expression, compared to the day one reference sample of monocytes/macrophages (expression level set to 1). The expression of the M2 marker IL-10 was diminished over time for all examined morphologies.

4.2. Human macrophages can adapt an elongated morphology on box-shaped 3D scaffolds

For further experiments, box-shaped scaffolds consisting of perfectly parallel and perpendicular fibers with pores ranging from 40 to 100 μm in both, x- and y-direction, were established (figures 3(a)–(e)). Based on the technical feasibilities of easy scaffold handling as well as controllable printing behavior, the optimal stacking height of the fibers was determined for each pore size and ranged from 20 to 60 layers (table 2). The PCL scaffolds exhibited a high flexibility as has been shown previously [44]. In addition, a precise stacking behavior of the fibers upon each other was achieved with a consistently rough surface topography of the individual fibers (figure 3(f)).

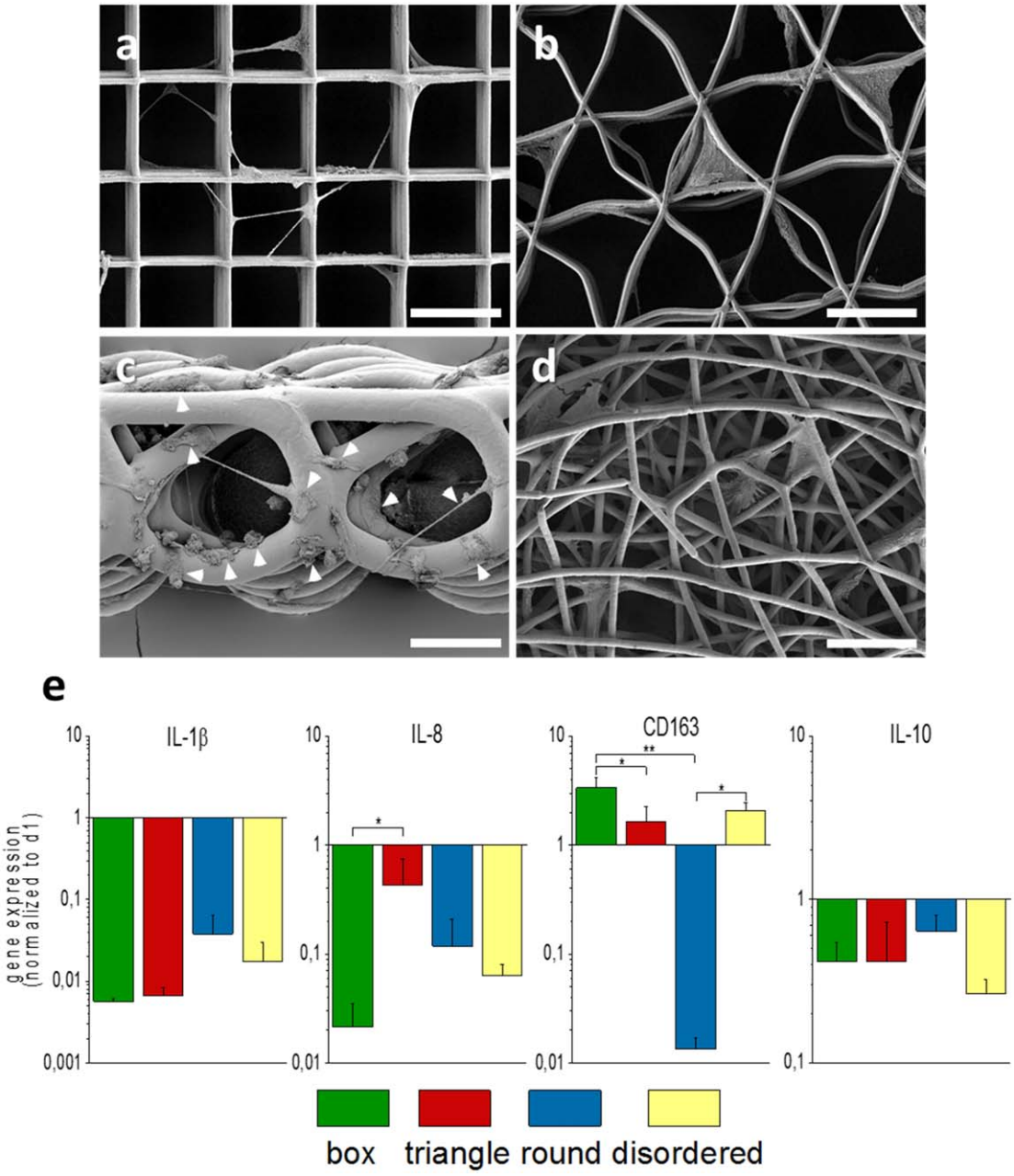

Figure 2. Morphology and gene expression profile of spontaneously differentiated macrophages on PCL MEW scaffolds with different geometries. The cellular morphology of macrophages cultivated for seven days was observed via SEM on scaffolds with a box-shaped (a), triangle-shaped (b), round-shaped (white arrowheads indicate diverse macrophage phenotypes) (c), and randomly disordered scaffold (d) geometry, scale bar = 50 μm. Gene expression analysis via qPCR (e) suggested spontaneous differentiation of macrophages on all tested scaffold geometries over time (compared to the reference sample (monocytes/macrophages at day 1 on the corresponding scaffold type)). While both M1-markers, IL-1β and IL-8, were decreased after cultivation on the scaffolds, the M2 markers, CD163 and IL-10, rather increased, except for the roundish geometry, or experienced only a mild reduction compared to day 1. The fold changes of gene expression are given as logarithmic values with the expression of the corresponding day 1 set to 1 (mean $\pm$ SD, $n = 3$). $^{*}p < 0.05$; $^{**}p < 0.01$.

SEM imaging after seven days of cultivation showed that macrophages were able to stretch along single fibers and bridge across pores, perpendicular as well as parallel fibers in each scaffold in a certain degree. (Figures 4(a)–(e)). With increasing pore size, more roundish as well as flattened cells were observed on the scaffold walls. Vice versa, higher numbers of elongated macrophages with long cellular extensions were detected on scaffolds with decreasing pore sizes. On scaffolds with a pore size of 40 μm more than 50% of the cells were elongated with an average length of about 80 μm. With increasing pore sizes, the number of elongated cells reduced down to 20% for the fiber distance of 100 μm. This was accompanied by an increase of rounded as well as flattened cells being neatly attached to the scaffold walls. The length of the

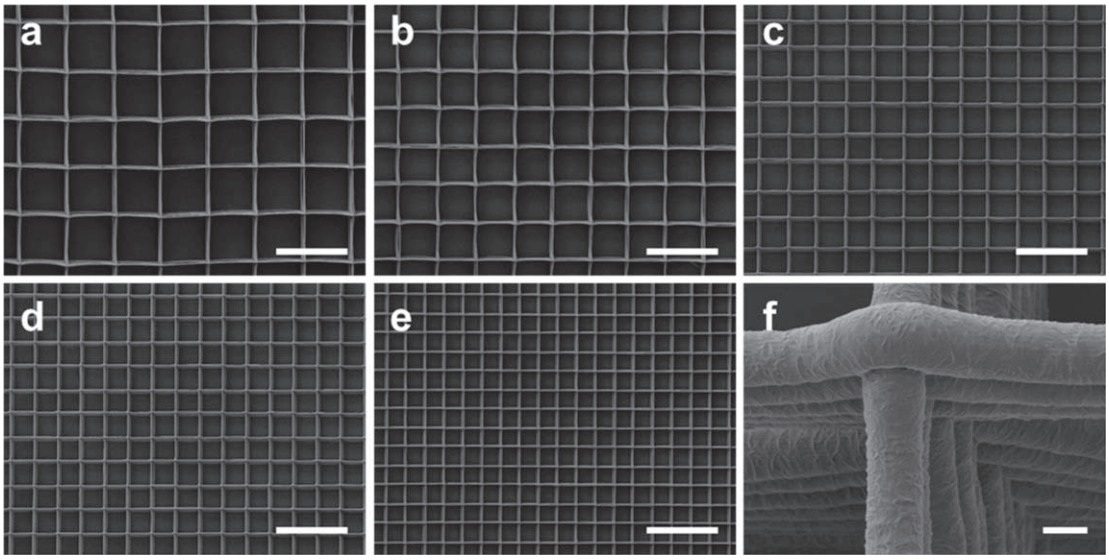

Figure 3. SEM images of the established, box-shaped PCL MEW scaffolds. Representative images of scaffolds with different pore sizes ((a): 100 μm, (b): 80 μm, (c): 60 μm; (d): 50 μm; (e): 40 μm) and different numbers of stacking layers in *x*- and *y*-direction ((a): 2 × 30, (b): 2 × 20; (c): 2 × 18; (d): 2 × 15; (e): 2 × 10 layers) with a fiber diameter of around 3 μm ;(f) (scaffold with 60 μm pore size and a stacking height of 2 × 18 layers) represent the highly precise stacking behavior of the fibers on top of each other. Scale bar = 150 μm (a)–(e) and 2 μm (f).

elongated cells did no longer significantly decrease from a pore size of 60 μm upwards and was maintained at an average of about 50 μm (figures 4(f), (g)).

On all tested scaffolds, similar amounts of DNA and thus cell numbers were determined at the examined time point, which excluded any cell density-associated bias on our analysis (figure S3).

4.3. Pore sizes of box-shaped scaffolds directs the spontaneous differentiation and phagocytic activity of human macrophages

The outcome of the spontaneous differentiation of monocyte-derived macrophages after seven days on scaffolds with varying pore sizes of 40–100 μm as well as on 2D PCL films was compared to macrophages cultured for one day on the corresponding scaffold/film type (figure 5).

Concerning the expression of the M1 markers IL-1β and IL-8, porous scaffolds triggered a significant downregulation compared to the 2D control. Among the different scaffold types, no significant expression differences were obtained. The expression of the M2 marker CD163 was significantly upregulated after cultivation of macrophages on scaffolds with a pore size of 40–60 μm. However, the larger the pore, the smaller was the augmentation of the CD163 gene expression, which even turned into a decrease for pores of 80 and 100 μm. In contrast, an elevated expression of the M2 markers CD206 and CD163 on scaffolds with a pore size of 40 μm and 50 μm was detected while increasing pore sizes diminished and even reverted the effect into a decline of gene expression for CD206 and CD163, respectively. Macrophages on the 2D control showed minimal up- or downregulation of the M2 macrophage differentiation markers over the time of seven days. Albeit, when considering the corresponding 2D reference sample, the IL-10 expression of macrophages was at a similar steady state level on 40 μm scaffolds and was further reduced on scaffolds with larger pores.

The IL-1β, IL-8, IL-6, and IL-10 cytokine release by macrophages was examined after three and seven days of cultivation on box-shaped scaffolds with varying pore sizes and on 2D PCL films (figure 6).

On all porous scaffolds, the release of IL-1β had declined after seven days. The cultivation on the 2D films did not affect the IL-1β release over time, which was constantly much higher than for samples derived from box-shaped scaffolds. Similar results, comparing 2D films and porous scaffolds, were ascertained for the release of IL-8. A significantly higher release of IL-6 was determined after three days of cultivation comparing the 2D control with scaffolds of 40 μm and 50 μm pore size, respectively. After seven days, macrophages on 40 μm scaffolds released the lowest amount of IL-6. Interestingly of all porous scaffolds, macrophages on scaffolds with 60 μm pores showed the highest release of IL-6 as well as of IL-1β after three days. The amount of released IL-10 was significantly higher after seven days on scaffolds with 40 μm pores compared to all other samples. Macrophages cultured on a 50 and 100 μm box-shaped scaffolds showed a significant decrease compared to the third day.

After seven days on either 3D scaffolds with pores ranging from 40 to 100 μm or on 2D PCL films as a control, the macrophages co-expressed the M2-specific surface markers CD206 and CD163 (figure 7). The immunofluorescence staining's depicted that both markers were higher expressed on scaffolds

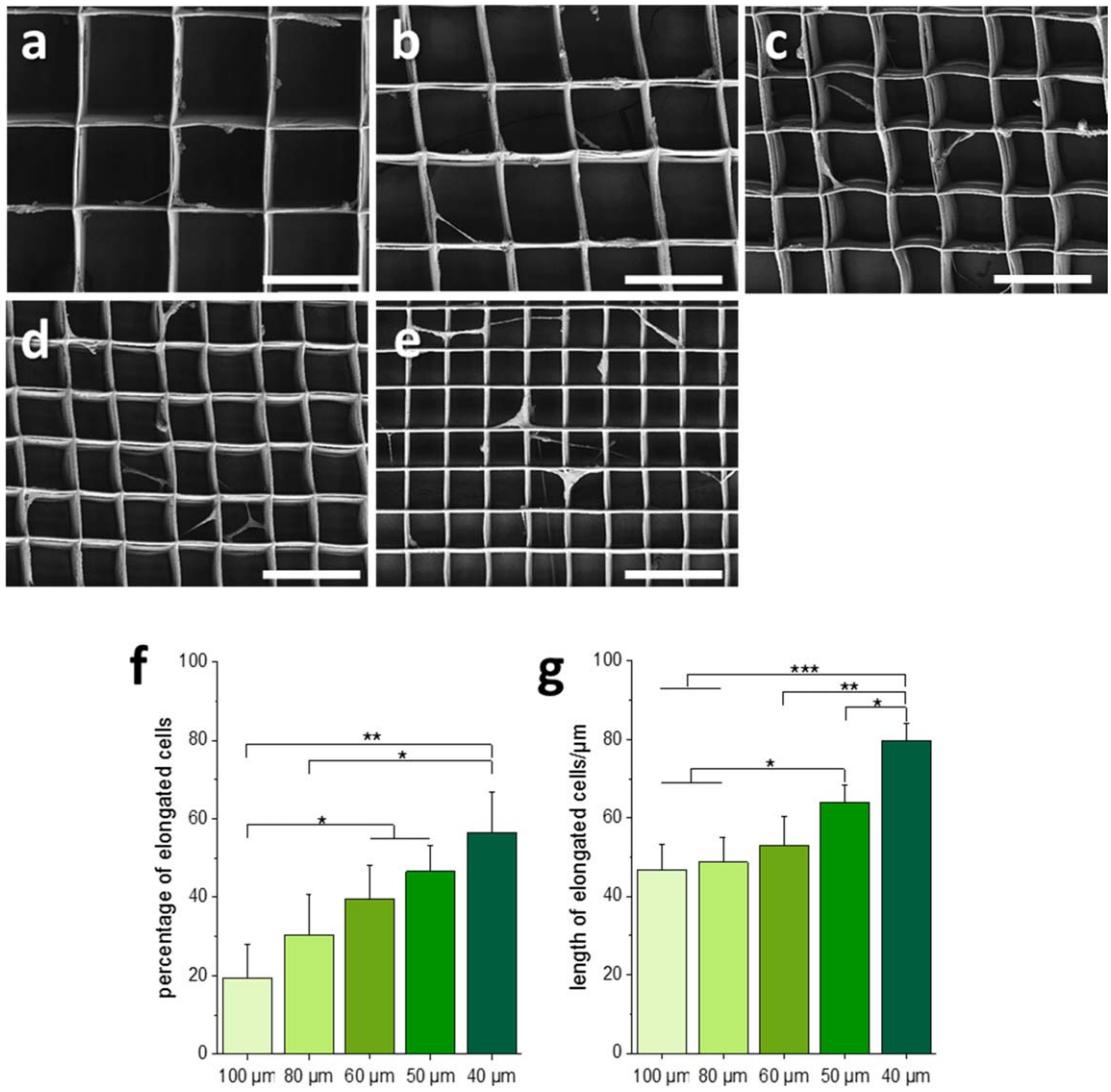

Figure 4. Cellular morphology and elongation behavior of macrophages after seven days of cultivation on 3D PCL MEW scaffolds. Macrophage morphology was examined via SEM on scaffolds with pore size of 100 μm (a), 80 μm (b), 60 μm (c) 50 μm (d), and 40 μm (e), scale bar = 100 μm. Cell numbers and the of percentage of elongated cells (f) as wells as the lengths of elongated cells (g) were determined via ImageJ (mean $\pm$ SD, $n = 3$), $^{*}p < 0.05$; $^{**}p < 0.01$, $^{***}p < 0.001$.

with pores of 40–60 μm than on scaffolds with 80 and 100 μm pores. Interestingly, elongated cells showed a more intense fluorescent staining.

The phagocytic activity of macrophages cultured on box-shaped scaffolds with varying pore sizes was augmented on day 1 (figure 8) when pore sizes increased from 40 to 80 μm as detected by the corresponding elevated bead uptake. Macrophage cultivation on the smallest pores of 40 and 50 μm showed an initial tendency on day 1 to decrease phagocytosis compared to 2D PCL films, while larger pores enhanced the bead uptake. Between pore sizes of 60 and 100 μm no further significant differences were observed. After a culture period of seven days, the number of phagocytosed beads was decreased significantly for pore sizes of up to 80 μm compared to 2D PCL films and even the largest pore size of 100 μm showed the same tendency. Thereby, no further differences between the varying 3D scaffold types were observed.

5. Discussion

Immediately after implantation, a biomaterial is exposed to the body's immune response, which particularly involves the action of macrophages arriving from the blood stream at the wound. An immediate but transient inflammation is important for healing. The transition of the polarization of macrophages into the regenerative, M2 type is, however, mandatory to overcome pronounced inflammatory response, and therefore is one of the major concerns in the fabrication and design of new biomaterials [4]. Besides biochemical modifications with cytokines or matrix proteins that may activate macrophage polarization [20, 45], macrophages are able to differentiate

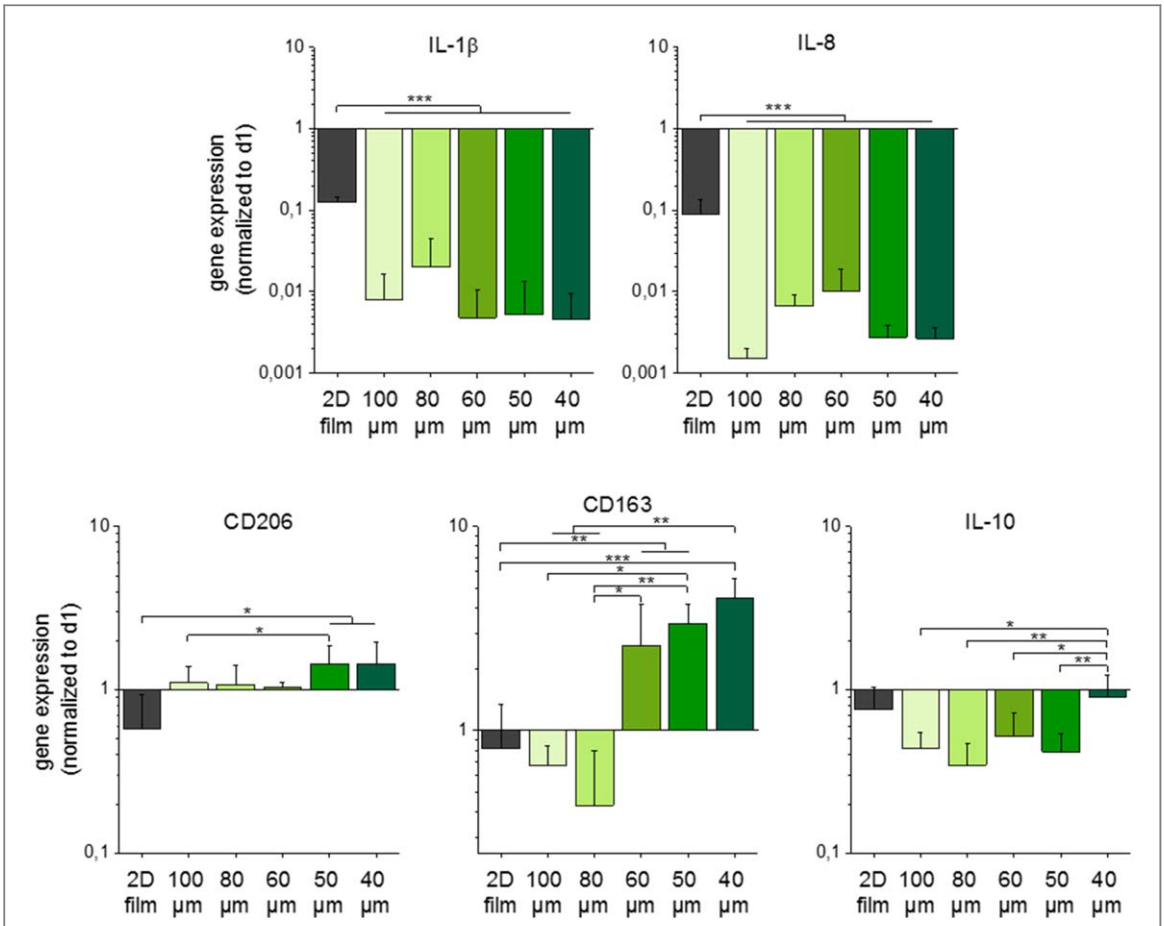

Figure 5. Gene expression profile of spontaneously differentiated macrophages on scaffolds with varying pore sizes. Gene expression was analyzed via qPCR. Spontaneous differentiation was observed on all tested scaffold with pores ranging from 40 to 100 μm. Gene expression of the M1 markers, IL-1β and IL-8, as wells as of the M2 markers, CD206, CD163, and IL-10, was examined. On scaffolds with smaller pores M2 marker expression was upregulated while all 3D scaffolds led to a pronounced reduction of M1 marker expression. (Mean $\pm$ SD, $n = 3$). $^{*}p < 0.05$; $^{**}p < 0.01$, $^{***}p < 0.001$.

spontaneously depending on mechanical cues like stiffness, topography or 3D geometry of the biomaterials [23, 25, 32, 46–49]. Hence, in the present study, we investigated the influence of different, precisely manufactured scaffold morphologies, produced via MEW, on the spontaneous differentiation of primary human monocyte-derived macrophages. Our investigations proved an association between pore sizes, cellular elongation, and polarization towards the regenerative M2 type of human macrophages.

We used the studies of Bryers *et al* [23] who demonstrated that a pHEMA sphere template scaffold with uniform and homogeneously distributed 34 μm pores supported murine macrophage polarization towards the M2 type, and Sussman *et al* [46], who demonstrated a reduction of the foreign body reaction by such scaffolds in a murine model of skin healing *in vivo*, as basis for our scaffold design rationale. For reproducible fabrication of such scaffolds in high quality, we advanced the MEW technique and successfully generated PCL scaffolds with regular inter-filament distances down to 40 μm. In contrast to the cast scaffolds mentioned above that only allow for a limited variety of pore shapes, we have also successfully established the production of scaffolds with different porous geometries via the precise and uniform deposition of individual PCL fibers.

Previously, polylactic acid scaffolds with triangular-like, diagonal pores triggered macrophages to polarize into an M2-like phenotype *in vitro,* which was accompanied by a reduced release of pro-inflammatory cytokines when compared to chitosan box-shaped, orthogonal pore constructs [24]. These diagonal ordered scaffolds were, however, prepared with conventional additive manufacturing technologies resulting in filament diameters of 75 $\pm$ 5 μm as well as inter-filament spacings of 165 $\pm$ 5 μm. Nonetheless, the comparison of chitosan scaffolds with diagonal and orthogonal structures with filament diameters of 250 $\pm$ 30 μm and spacings of 380 $\pm$ 60 μm and 600 $\pm$ 93 μm, respectively, led to no significantly differences. Consequently, the examination of changes in macrophage behavior within a suitable 3D environment, excluding the effect of the material itself, was not properly possible. In addition, it should be considered that human macrophages, in a roundish phenotype, can only reach a cell diameter of up to 20–30 μm [50]. Therefore, fiber diameters could strongly

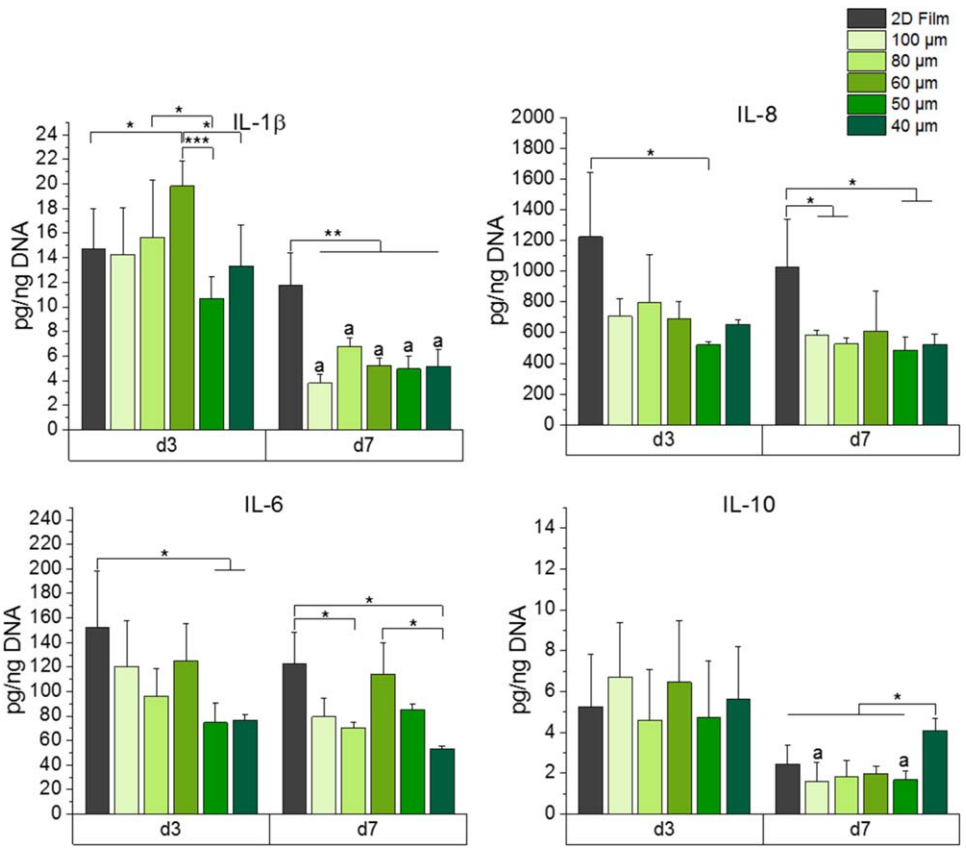

Figure 6. Cytokine release of spontaneously differentiated macrophages. The cytokine release of IL-1β, IL-8, IL-6, and IL-10 was measured using supernatants of macrophages cultivated on a 2D PCL film and 3D PCL MEW scaffolds with pores ranging from 40 to 100 μm. The amounts of released cytokines were normalized to the DNA content of the corresponding sample. (mean $\pm$ SD, $n = 3$). $^{*}p < 0.05$; $^{**}p < 0.01$, $^{***}p < 0.001$; $^{a}p < 0.05$ versus d1, same culture condition.

affect the recognition of scaffolds as 3D or 2D environment. Considering this former study, we produced PCL scaffolds with triangle- and box-shaped morphology, however with distinct smaller pore sizes and fiber diameters. Box-shaped MEW scaffolds have already been described in previous studies [23, 37, 39, 51]. Here, the manufacturing procedure was improved from the perspective of scaffolds with significantly smaller pores, with the previously smallest pore size described being 90 μm [39]. Furthermore, we have successfully established the production of scaffolds with cylinder-like pores from PCL fibers to assess the role of biomaterial surface curvature. These scaffolds made of PCL were limited to a larger pore (around 70 μm) and fiber (around 18 μm) diameter. The pro-inflammatory cytokine release of macrophages on cylindrical pores diminished over time, but the concurrent decrease of the anti-inflammatory cytokine release rather hinted at an overall non-polarized macrophage type. This is in accordance with the presence of a broad range of different cell morphologies on these constructs (figure 2(c)). We assume that the flattened and the spherical cell morphology on the round-shaped scaffolds results from the larger fiber diameter. Thus, the comparably small cells could be hindered to recognize the 3D topography of the entire scaffolds. This would rather restrict them to interact with their immediate pericellular environment, i.e. only with the surface of a single fiber. To allow for better comparison of our newly established, highly ordered scaffolds with previous studies using random scaffold geometries [52, 53], the MEW procedure was additionally adjusted to produce randomly disordered scaffolds that mimic electrospun fiber constructs.

As concluded from our gene expression analyses, the most promising setup for the support of spontaneous differentiation towards the M2 type are the box-shaped scaffolds. Here, macrophages showed the highest expression of the M2-specific surface marker CD163 compared to all other scaffold types. Furthermore, both tested M1 markers (IL-1β, IL-8) were strongly downregulated to the lowest levels of all scaffolds. This is in accordance with the study of McWorther *et al* (2013) and Wang *et al* (2016), who proved an elongated phenotype to trigger murine macrophages into an M2-like polarization *in vitro* and *in vivo* [27, 28].

Guided by these outcomes, we focused on the box-shaped MEW scaffolds and to investigate the influence of these porous scaffolds and their different pore sizes on macrophage polarization potential. This is the first time that MEW scaffolds with a defined low pore size of 40 μm and excellent stacking quality resulting in highly ordered structures have been produced. As for

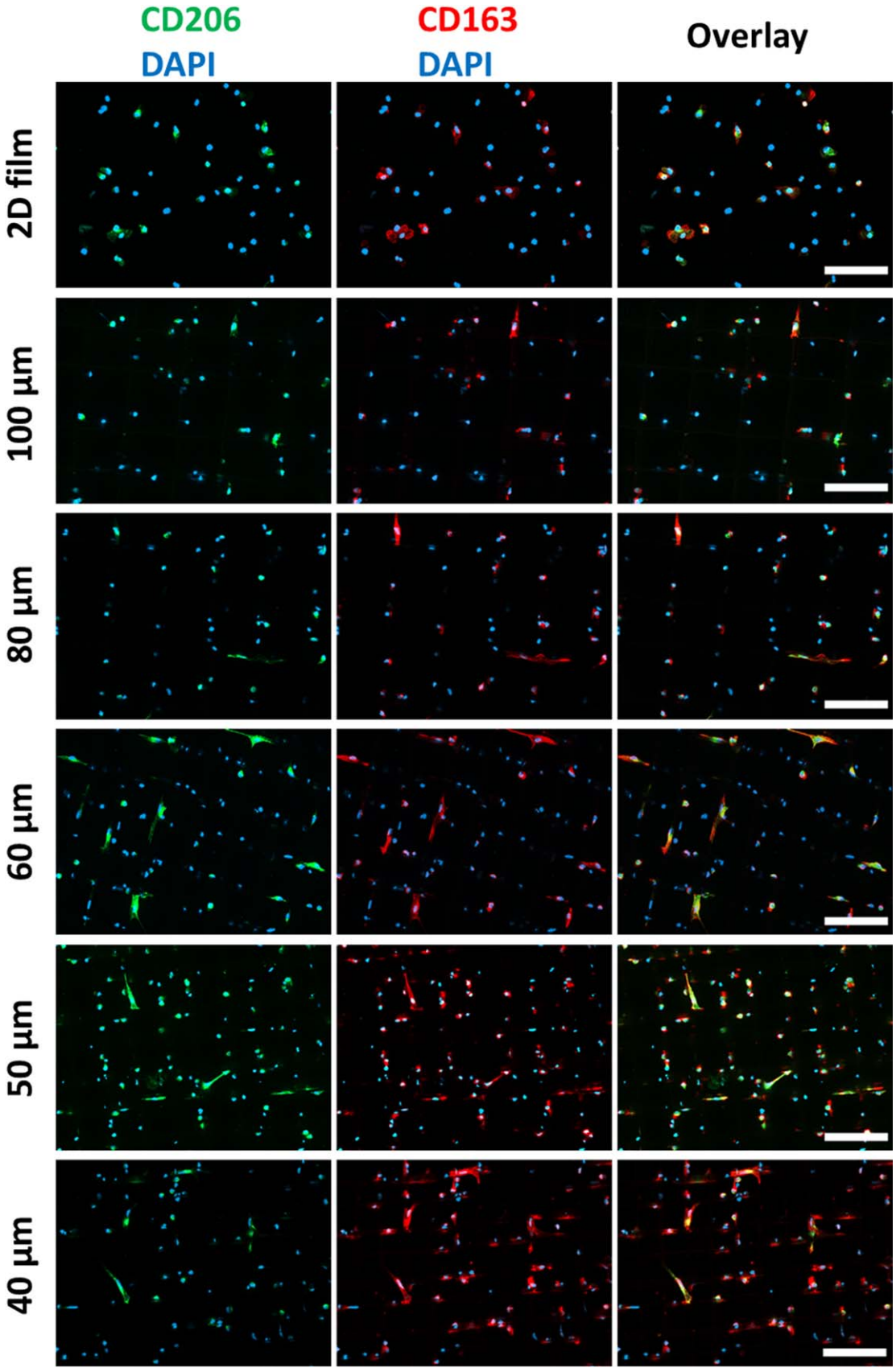

Figure 7. Immunofluorescent staining of the M2-characteristic surface markers CD206 and CD163. On melt-electrowritten 3D scaffolds with varying pore sizes from 40 to 100 μm, cultivated macrophages were stained against CD206 (green, left panel) and CD163 (red, mid panel) after seven days of spontaneous differentiation. The overlay of both channels is shown in the right panel. For counterstaining of the nuclei, DAPI (blue) was used. Staining with the appropriate isotype controls was negative and guaranteed the specificity of the antibodies used (figure S3). Scale bar = 100 μm.

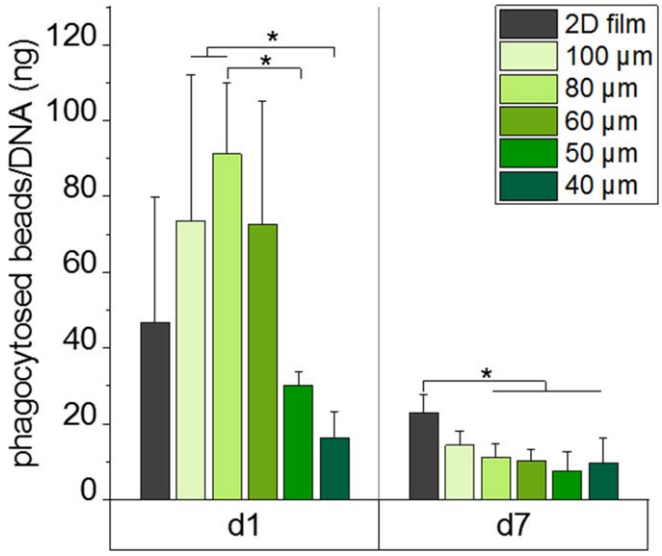

Figure 8. Phagocytic activity of macrophages cultivated on 3D MEW scaffolds with pores ranging from 40 to 100 μm. The phagocytic activity of macrophages cultivated on 3D PCL MEW scaffolds for one and seven days was detected via the uptake of fluorescent beads counted via fluorescence microscopy and normalized to the DNA content of the corresponding scaffold. After one day of cultivation higher phagocytic activity was observed on scaffolds with pore sizes of 60–100 μm compared to scaffolds with smaller pores. After seven days, a significant decrease of phagocytic activity for the cultivation on porous scaffolds was detected. (Mean $\pm$ SD, $n = 3$.) $^{**}p < 0.01$; $^{***}p < 0.001$.

all our defined pore sizes of 40, 50, 60, 80, and 100 μm, our manufacturing procedure outperformed previously described techniques regarding the accuracy and reproducibility of fiber deposition. In particular, this was a prerequisite to perform the biological experiments within this study, since it enabled the consistent immunological evaluation of the scaffold geometries.

As smaller pores for box-shaped scaffolds supported the stretched and elongated M2-like macrophage type (figure 4), we hypothesize that smaller pore sizes, separated by walls, built of relatively thin (2–3 μm) fibers prompt the cells to interact with the scaffold at several sites. In addition, smaller pore sizes appear to facilitate the formation of elongated macrophages, since the cells can more easily bridge the gaps between the fibers unlike on scaffolds with 80 or 100 μm pore sizes. To the best of our knowledge, we are the first to put pore sizes of highly ordered scaffolds into context with the elongation behavior of macrophages.

M2-specific markers (CD163, CD206, and IL-10; figures 5–7) were higher expressed and released on scaffolds when using smaller pores and decreased with increasing pore size. We assume, that especially the higher CD163 expression correlates with the higher percentage and length of elongated macrophages which is in good accordance with previous studies [25, 26] using murine cells in a structured 2D environment and hence can be transferred to the events in human primary macrophages in 3D. IL-10, a main anti-inflammatory cytokine [54] was released in significantly higher amounts especially for macrophages cultured on box-shaped scaffolds with a 40 μm pores. Furthermore, the particularly intense staining of elongated cells for these M2 markers indicated that this morphology change induced by smaller pore sizes increases the differentiation towards the M2 type. The appearance of higher cell numbers on smaller pore scaffolds than on larger pore size scaffolds does not seem to fit the DNA determination results (figure S3). We assume that this effect could be due to an inhomogeneous cell seeding. In addition, we hypothesize that roundish cells, such as on larger pores, do not adhere as firmly to the scaffolds as elongated macrophages on smaller pores, and thus, this leads to cell loss through the extensive washing steps required for immunostaining.

As the gene expression of the tested M1 markers (IL-1β, IL-8) was strongly downregulated on all square porous scaffolds with significant differences to the 2D control, which showed a slighter decrease, this suggest an anti-inflammatory differentiation effect of porous MEW scaffolds over the time period of seven days. Additionally, the 2D PCL control showed a larger potential for stimulating the release of pro-inflammatory cytokines over the whole culture period, which is in accordance to previous studies, where flat films led to an increased formation of fibrous capsules [32], or an enhanced pro-inflammatory outcome [52] compared to porous 3D electrospun fiber scaffolds. Moreover, based on the decreased release of IL-6 and IL-8 on scaffolds with 40 and 50 μm pores on day three, we assume that scaffolds with smaller pores amplify the anti-inflammatory response.

The phagocytosis of pathogens, but also of foreign bodies is a main task of macrophages. In literature it is controversially discussed, whether the phagocytic activity is induced by the M1 [55]- or the M2 type

[56, 57] of macrophages. However, these studies were conducted in a conventional 2D culture and a transfer of this knowledge to 3D culture setups is hardly possible. One study described previously an increased phagocytic activity of M1-induced macrophages in a 3D nano-scaffold based on collagen and chitosan [58] that correlates slightly with our findings. With a decrease of pore size and especially on scaffolds with 40 and 50 μm, the initial phagocytotic activity was significantly lower compared to scaffolds with larger pores (figure 8). Based on our results of a lower initial pro-inflammatory response on scaffolds with smaller pores we assume, that this also led to a decreased phagocytic activity at day one. Therefore, we would set an increased phagocytosis in context with a rather pro-inflammatory response. Moreover, concordantly with the reduced pro-inflammatory cytokine release, less phagocytic activity appeared on the 3D scaffolds, compared to the 2D control, after seven days, which further highlighted the benefits of porous scaffolds.

Our findings suggest that porous scaffolds with a pore size of 40 μm are beneficial for enhancing both the elongation and the polarization of human macrophages towards the M2 type. However, an absolute guarantee that this can be translated to *in vivo* can not be given. Previous studies evaluated the *in vivo* and *in vitro* comparison of different tissue engineering aspects [59, 60], partly, with a poor outcome. Nonetheless, the *in vitro* assessment of the immune response is important and can minimize the risk of patients [61]. Moreover, studies have already shown that the macrophage response investigated *in vitro* could also be transferred to *in vivo* processes [28, 59]. Therefore, we are convinced that our findings can improve the design of new biomaterials and have the potential to be transferable to *in vivo* processes.

6. Conclusion

In this study, we demonstrate that fiber scaffolds with precisely controlled pore sizes between 40 and 100 μm lead to elongation of adherent primary human macrophages, accompanied by a polarization towards the M2 type. This effect was most pronounced for the smallest pores of 40 μm. The down-regulation of pro-inflammatory markers and the concomitant up-regulation of anti-inflammatory factors as well as the cell elongation were thereby increased with decreasing pore size. We thus show that the so far not achieved elongation driven polarization of human macrophages towards a regenerative macrophage type can be obtained by 3D scaffolds, provided that the scaffolds geometry can be controlled precisely in cellular dimensions. These findings open a perspective to generate immunomodulatory pro-healing scaffolds solely through structural control. Hence, the overall aim should be to induce macrophages elongation and thereby enhance the polarization towards the M2 type. This strategy can be applied for future biomaterial designs to improve tissue regeneration and wound healing, especially for biomaterial membranes and as scaffolds for thin tissues.

Acknowledgments

The authors appreciate the European Research Council (ERC) (consolidator grant Design2Heal, contract #617989) for financial support as well as the German Research Foundation (DFG) State Major Instrumentation Programme for funding the Zeiss Crossbeam CB 340 SEM (INST 105022/58-1 FUGG). The authors thank Daimon Hall (carbonandneon.com) for support with graphical design.

Author contributions

T T, C B, K S, and J G conceived the research; T T and C B performed the experiments and analyzed the data (T T: biological experiments; C B: MEW and characterization of scaffolds); A H and P D provided support for MEW; T T and C B prepared the manuscript in consultation with T S, K S, A H, P D and J G; K S and T S help supervising the project.

Competing interests

The authors declare that they have no competing interests.

ORCID iDs

Tina Tylek https://orcid.org/0000-0003-1102-8431
Carina Blum https://orcid.org/0000-0003-2251-2114
Jürgen Groll https://orcid.org/0000-0003-3167-8466

References

[1] Vishwakarma A, Bhise N S, Evangelista M B, Rouwkema J, Dokmeci M R, Ghaemmaghami A M, Vrana N E and Khademhosseini A 2016 Engineering immunomodulatory biomaterials to tune the inflammatory response *Trends Biotechnol.* **34** 470–82
[2] Anderson J M, Rodriguez A and Chang D T 2008 Foreign body reaction to biomaterials *Semin. Immunol.* **20** 86–100
[3] Anderson J M 2001 Biological responses to materials *Annu. Rev. Mater. Res.* **31** 81–110
[4] Sridharan R, Cameron A R, Kelly D J, Kearney C J and O'Brien F J 2015 Biomaterial based modulation of macrophage polarization: a review and suggested design principles *Mater. Today* **18** 313–25
[5] Mantovani A, Biswas S K, Galdiero M R, Sica A and Locati M 2013 Macrophage plasticity and polarization in tissue repair and remodelling *J. Pathol.* **229** 176–85
[6] Mantovani A, Sica A, Sozzani S, Allavena P, Vecchi A and Locati M 2004 The chemokine system in diverse forms of macrophage activation and polarization *Trends Immunol.* **25** 677–86

[7] Recalcati S, Locati M, Marini A, Santambrogio P, Zaninotto F, De Pizzol M, Zammataro L, Girelli D and Cairo G 2010 Differential regulation of iron homeostasis during human macrophage polarized activation *Eur. J. Immunol.* **40** 824–35

[8] Brown B N, Ratner B D, Goodman S B, Amar S and Badylak S F 2012 Macrophage polarization: an opportunity for improved outcomes in biomaterials and regenerative medicine *Biomaterials* **33** 3792–802

[9] Koh T J and DiPietro L A 2011 Inflammation and wound healing: the role of the macrophage *Expert Rev. Mol. Med.* **13** e23

[10] Italiani P and Boraschi D 2014 From Monocytes to M1/M2 Macrophages: Phenotypical vs. Functional Differentiation *Frontiers Immunol.* **5** 514

[11] Gordon S 2003 Alternative activation of macrophages *Nat. Rev. Immunol.* **3** 23–35

[12] Martinez F O, Sica A, Mantovani A and Locati M 2008 Macrophage activation and polarization *Frontiers Biosci.* **13** 453–61

[13] Gordon S and Martinez F O 2010 Alternative activation of macrophages: mechanism and functions *Immunity* **32** 593–604

[14] Kajahn J, Franz S, Rueckert E, Forstreuter I, Hintze V, Moeller S and Simon J C 2012 Artificial extracellular matrices composed of collagen I and high sulfated hyaluronan modulate monocyte to macrophage differentiation under conditions of sterile inflammation *Biomatter* **2** 226–36

[15] Brown B N, Londono R, Tottey S, Zhang L, Kukla K A, Wolf M T, Daly K A, Reing J E and Badylak S F 2012 Macrophage phenotype as a predictor of constructive remodeling following the implantation of biologically derived surgical mesh materials *Acta Biomater.* **8** 978–87

[16] Huleihel L *et al* 2017 Macrophage phenotype in response to ECM bioscaffolds *Semin. Immunol.* **29** 2–13

[17] Cheng H, Fan X, Wu C, Wang X, Wang L-J, Loh X J, Li Z and Wu Y-L 2019 Cyclodextrin-based star-like amphiphilic cationic polymer as a potential pharmaceutical carrier in macrophages *Macromol. Rapid Commun.* **40** 1800207

[18] Sun H, Wang X, Hu X, Yu W, You C, Hu H and Han C 2012 Promotion of angiogenesis by sustained release of rhGM-CSF from heparinized collagen/chitosan scaffolds *J. Biomed. Mater. Res.* B **100** 788–98

[19] Chen J, Li M, Yang C, Yin X, Duan K, Wang J and Feng B 2018 Macrophage phenotype switch by sequential action of immunomodulatory cytokines from hydrogel layers on titania nanotubes *Colloids Surf.* B **163** 336–45

[20] Yang C L, Sun Y H, Yu W H, Yin X Z, Weng J and Feng B 2018 Modulation of macrophage phenotype through controlled release of interleukin-4 from gelatine coatings on titanium surfaces *Eur. Cell Mater.* **36** 15–29

[21] Wistlich L, Kums J, Rossi A, Heffels K-H, Wajant H and Groll J 2017 Multimodal bioactivation of hydrophilic electrospun nanofibers enables simultaneous tuning of cell adhesivity and immunomodulatory effects *Adv. Funct. Mater.* **27** 1702903

[22] Meli V S, Veerasubramanian P K, Atcha H, Reitz Z, Downing T L and Liu W F 2019 Biophysical regulation of macrophages in health and disease *J. Leukoc Biol.* **106** 283–99

[23] Bryers J D, Giachelli C M and Ratner B D 2012 Engineering biomaterials to integrate and heal: the biocompatibility paradigm shifts *Biotechnol. Bioeng.* **109** 1898–911

[24] Almeida C R, Serra T, Oliveira M I, Planell J A, Barbosa M A and Navarro M 2014 Impact of 3D printed PLA- and chitosan-based scaffolds on human monocyte/macrophage responses: unraveling the effect of 3D structures on inflammation *Acta Biomater.* **10** 613–22

[25] Chen S, Jones J A, Xu Y, Low H Y, Anderson J M and Leong K W 2010 Characterization of topographical effects on macrophage behavior in a foreign body response model *Biomaterials* **31** 3479–91

[26] McWhorter F Y, Davis C T and Liu W F 2015 Physical and mechanical regulation of macrophage phenotype and function *Cell. Mol. Life Sci.* **72** 1303–16

[27] McWhorter F Y, Wang T, Nguyen P, Chung T and Liu W F 2013 Modulation of macrophage phenotype by cell shape *Proc. Natl Acad. Sci. USA* **110** 17253–8

[28] Wang T, Luu T U, Chen A, Khine M and Liu W F 2016 Topographical modulation of macrophage phenotype by shrink-film multi-scale wrinkles *Biomater Sci.* **4** 948–52

[29] Toniolo A, Fadini G P, Tedesco S, Cappellari R, Vegeto E, Maggi A, Avogaro A, Bolego C and Cignarella A 2015 Alternative activation of human macrophages is rescued by estrogen treatment *in vitro* and impaired by menopausal status *J. Clin. Endocrinol. Metab.* **100** E50–8

[30] Yang Y *et al* 2017 Macrophage-derived foam cells impair endothelial barrier function by inducing endothelial-mesenchymal transition via CCL-4 *Int. J. Mol. Med.* **40** 558–68

[31] Bartneck M, Heffels K H, Pan Y, Bovi M, Zwadlo-Klarwasser G and Groll J 2012 Inducing healing-like human primary macrophage phenotypes by 3D hydrogel coated nanofibres *Biomaterials* **33** 4136–46

[32] Cao H, McHugh K, Chew S Y and Anderson J M 2010 The topographical effect of electrospun nanofibrous scaffolds on the *in vivo* and *in vitro* foreign body reaction *J. Biomed. Mater. Res.* A **93** 1151–9

[33] Hutmacher D W and Dalton P D 2011 Melt Electrospinning *Chem.—Asian J.* **6** 44–56

[34] Dalton P D 2017 Melt electrowriting with additive manufacturing principles *Curr. Opin. Biomed. Eng.* **2** 49–57

[35] Muerza-Cascante M L, Haylock D, Hutmacher D W and Dalton P D 2015 Melt electrospinning and its technologization in tissue engineering *Tissue Eng.* B **21** 187–202

[36] McMaster R *et al* 2019 Tailored melt electrowritten scaffolds for the generation of sheet-like tissue constructs from multicellular spheroids *Adv. Healthcare Mater.* **8** 1801326

[37] Hrynevich A, Elci B S, Haigh J N, McMaster R, Youssef A, Blum C, Blunk T, Hochleitner G, Groll J and Dalton P D 2018 Dimension-based design of melt electrowritten scaffolds *Small* **14** 1800232

[38] Youssef A, Hollister S J and Dalton P D 2017 Additive manufacturing of polymer melts for implantable medical devices and scaffolds *Biofabrication* **9** 012002

[39] Hochleitner G, Jungst T, Brown T D, Hahn K, Moseke C, Jakob F, Dalton P D and Groll J 2015 Additive manufacturing of scaffolds with sub-micron filaments via melt electrospinning writing *Biofabrication* **7** 035002

[40] Wunner F M, Wille M L, Noonan T G, Bas O, Dalton P D, De-Juan-Pardo E M and Hutmacher D W 2018 Melt electrospinning writing of highly ordered large volume scaffold architectures *Adv. Mater.* **30** e1706570

[41] Brown T D, Edin F, Detta N, Skelton A D, Hutmacher D W and Dalton P D 2014 Melt electrospinning of poly(ε-caprolactone) scaffolds: phenomenological observations associated with collection and direct writing *Mater. Sci. Eng.* C **45** 698–708

[42] Hochleitner G, Youssef A, Hrynevich A, Haigh Jodie N, Jungst T, Groll J and Dalton Paul D 2016 Fibre pulsing during melt electrospinning writing *BioNanoMaterials* **17** 159

[43] Tylek T, Schilling T, Schlegelmilch K, Ries M, Rudert M, Jakob F and Groll J 2019 Platelet lysate outperforms FCS and human serum for co-culture of primary human macrophages and hMSCs *Sci. Rep.* **9** 3533

[44] Blum C, Schlegelmilch K, Schilling T, Shridhar A, Rudert M, Jakob F, Dalton P, Blunk T, Flynn L and Groll J 2019 Extracellular matrix-modified fiber scaffolds as a pro-adipogenic mesenchymal stromal cell delivery platform *ACS Biomater. Sci. Eng.* **5** 6655–66

[45] Zaveri T D, Lewis J S, Dolgova N V, Clare-Salzler M J and Keselowsky B G 2014 Integrin-directed modulation of macrophage responses to biomaterials *Biomaterials* **35** 3504–15

[46] Sussman E M, Halpin M C, Muster J, Moon R T and Ratner B D 2014 Porous implants modulate healing and induce shifts in local macrophage polarization in the foreign body reaction *Ann. Biomed. Eng.* **42** 1508–16

[47] Patel N R *et al* 2012 Cell elasticity determines macrophage function *PLoS One* **7** e41024

[48] Paul N E, Skazik C, Harwardt M, Bartneck M, Denecke B, Klee D, Salber J and Zwadlo-Klarwasser G 2008 Topographical control of human macrophages by a regularly microstructured polyvinylidene fluoride surface *Biomaterials* **29** 4056–64
[49] Bota P C, Collie A M, Puolakkainen P, Vernon R B, Sage E H, Ratner B D and Stayton P S 2010 Biomaterial topography alters healing in vivo and monocyte/macrophage activation in vitro *J. Biomed. Mater. Res.* A **95** 649–57
[50] Krombach F, Münzing S, Allmeling A M, Gerlach J T, Behr J and Dörger M 1997 Cell size of alveolar macrophages: an interspecies comparison *Environ. Health Perspect.* **105** 1261–3
[51] Bertlein S, Hikimoto D, Hochleitner G, Hümmer J, Jungst T, Matsusaki M, Akashi M and Groll J 2018 Development of endothelial cell networks in 3D Tissues by combination of melt electrospinning writing with cell-accumulation technology *Small* **14** 1701521
[52] Saino E, Focarete M L, Gualandi C, Emanuele E, Cornaglia A I, Imbriani M and Visai L 2011 Effect of electrospun fiber diameter and alignment on macrophage activation and secretion of proinflammatory cytokines and chemokines *Biomacromolecules* **12** 1900–11
[53] Hixon Katherine R, Dunn Andrew J, Flores R, Minden-Birkenmaier Benjamin A, Kalaf Emily A G, Shornick Laurie P and Sell Scott A 2017 Using electrospun scaffolds to promote macrophage phenotypic modulation and support wound healing *Electrospinning* **1** 31
[54] Couper K N, Blount D G and Riley E M 2008 IL-10: the master regulator of immunity to infection *J. Immunol.* **180** 5771–7
[55] Zhang M *et al* 2016 Anti-CD47 treatment stimulates phagocytosis of glioblastoma by M1 and M2 polarized macrophages and promotes M1 polarized macrophages *in vivo* *PLoS One* **11** e0153550
[56] Schulz D, Severin Y, Zanotelli V R T and Bodenmiller B 2019 In-depth characterization of monocyte-derived macrophages using a mass cytometry-based phagocytosis assay *Sci. Rep.* **9** 1925
[57] Lingnau M, Hoflich C, Volk H D, Sabat R and Docke W D 2007 Interleukin-10 enhances the CD14-dependent phagocytosis of bacteria and apoptotic cells by human monocytes *Hum. Immunol.* **68** 730–8
[58] Mahmoudzadeh A, Mohsenifar A and Rahmani-Cherati T 2016 Collagen-chitosan 3D nano-scaffolds effects on macrophage phagocytosis and pro-inflammatory cytokine release *J. Immunotoxicol* **13** 526–34
[59] Mauney J R, Jaquiery C, Volloch V, Heberer M, Martin I and Kaplan D L 2005 *In vitro* and *in vivo* evaluation of differentially demineralized cancellous bone scaffolds combined with human bone marrow stromal cells for tissue engineering *Biomaterials* **26** 3173–85
[60] Billström G *et al* 2016 A surprisingly poor correlation between *in vitro* and *in vivo* testing of biomaterials for bone regeneration: results of a multicentre analysis *Eur. Cells Mater.* **31** 312–22
[61] Lock A, Cornish J and Musson D S 2019 The role of *in vitro* immune response assessment for biomaterials *J. Funct. Biomater.* **10** 31